

A High-Performance Graphene Oxide-Doped Ion Gel as Gel Polymer Electrolyte for All-Solid-State Supercapacitor Applications

Xi Yang, Fan Zhang, Long Zhang, Tengfei Zhang, Yi Huang, and Yongsheng Chen*

A high-performance graphene oxide (GO)-doped ion gel (P(VDF-HFP)-EMIMBF₄-GO gel) is prepared by exploiting copolymer (poly(vinylidene fluoride-hexafluoro propylene), P(VDF-HFP)) as the polymer matrix, ionic liquid (1-ethyl-3-methylimidazolium tetrafluoroborate, EMIMBF₄) as the supporting electrolyte, and GO as the ionic conducting promoter. This GO-doped ion gel demonstrates significantly improved ionic conductivity compared with that of pure ion gel without the addition of GO, due to the homogeneously distributed GO as a 3D network throughout the GO-doped ion gel by acting like a ion “highway” to facilitate the ion transport. With the incorporation of only a small amount of GO (1 wt%) in ion gel, there has been a dramatic improvement in ionic conductivity of about 260% compared with that of pure ion gel. In addition, the all-solid-state supercapacitor is fabricated and measured at room temperature using the GO-doped ion gel as gel polymer electrolyte, which demonstrates more superior electrochemical performance than the all-solid-state supercapacitor with pure ion gel and the conventional supercapacitor with neat EMIMBF₄, in the aspect of smaller internal resistance, higher capacitance performance, and better cycle stability. These excellent performances are due to the high ionic conductivity, excellent compatibility with carbon electrodes, and long-term stability of the GO-doped ion gel.

1. Introduction

Nowadays, portable electronic devices (e.g., mobile phones, notebooks, and cameras) are becoming more and more demanding for multifunctional energy storage devices being small, thin, lightweight, and flexible.^[1,2] Therefore, for the special configuration design and fabrication of novel energy storage devices, a thin and flexible layer of polymer electrolyte is considered to be the most effective geometry because of the intrinsic properties of polymer electrolyte, such as thin-film forming ability, flexibility as well as the relatively high ionic conductivity

and wide electrochemical window.^[3,4] Compared with the conventional energy storage devices using liquid electrolytes, all-solid-state energy storage devices based on polymer electrolytes don't require high standard safety encapsulation materials and thus their geometry shape is variable, which may bring new design opportunities for energy storage devices in the future wearable electronics field.^[5,6]

Conventional polymer electrolytes include solid polymer electrolytes (SPEs) (solid solutions of electrolyte salts in polymers) and gel polymer electrolytes (GPEs) (“ion gels” of electrolytes trapped in polymers).^[3] However, because of the ultralow ionic conductivity of SPEs at room temperature,^[6] great efforts are being dedicated to prepare high-performance GPEs for the all-solid-state energy storage device applications.^[7–14]

In order to prepare high-performance GPEs, several promising supporting electrolyte/polymer matrix systems, named “ion gels”,^[4] have been explored in recent years. Primarily, several polymer matrix materials have been developed and investigated for preparing high-performance ion gels,^[15] including poly(ethylene oxide) (PEO), poly(vinyl alcohol) (PVA), poly(methyl methacrylate) (PMMA), poly(acrylonitrile) (PAN), poly(vinylidene fluoride) (PVDF), and copolymer poly(vinylidene fluoride-hexafluoro propylene) (P(VDF-HFP)). Among these polymers, copolymer P(VDF-HFP), with crystalline parts (PVDF) to maintain the mechanical property and amorphous parts (PHFP) to trap the liquid electrolyte,^[15,16] has been demonstrated to exhibit high performance in ion gel systems.

Furthermore, the traditional supporting electrolytes in ion gel systems, including aqueous and organic supporting electrolytes, generally consist of polar solvents and electrolyte salts in polymer matrixes,^[13] which have some critical problems, such as volatility and/or flammability when solvents are used in all-solid-state energy storage devices in a severe temperature range.^[17–19] Ionic liquids (ILs) are molten salts that remain in liquid state at room temperature and comprised of dissociated ions with no intervening solvent, which can be used as electrolytes without the addition of any salt since its intrinsic ionic conductivity.^[20] ILs have the unique properties as supporting electrolytes compared with other supporting electrolytes, such

X. Yang, F. Zhang, L. Zhang, T. F. Zhang,
Prof. Y. Huang, Prof. Y. S. Chen
Key Laboratory of Functional Polymer Materials
and Centre of Nanoscale Science and Technology
Institute of Polymer Chemistry
College of Chemistry
Nankai University
300071, Tianjin, China
E-mail: yschen99@nankai.edu.cn



DOI: 10.1002/adfm.201203556

as non-flammability, negligible vapor pressure, high operating voltage, and excellent electrochemical/thermal stability.^[15] Therefore, using ILs as a substitute for conventional supporting electrolytes has been of great interest for ion gel systems.^[4,19,21,22]

Moreover, for the purpose of further improving the ionic conductivity of ion gels, adding an inorganic material to ion gels has been demonstrated as one of the most favorable routes. These additional materials can be either ionic conductive (e.g., zeolites) or neutral (e.g., Al₂O₃, TiO₂, SiO₂, etc.).^[23–25] The reciprocity of additional materials and polymer matrixes will influence the aggregated state of polymer in ion gels and improve the ionic conductivity. Therefore, the effect on ionic conductivity is highly dependent on the specific surface area (SSA), Lewis acid and surface chemistry characteristics of these additional materials.^[6] Graphene oxide (GO), a single-layer of graphite oxide with ultrahigh SSA and abundant oxygen-containing functional groups,^[26–31] should be a favorable additional material to improve the ionic conductivity of ion gels. However, although the approach of using carbon nanofillers in polymer electrolytes has shown a remarkable improvement on ionic conductivity^[32,33] and graphene was widely used as electrode materials for supercapacitor applications,^[34–39] the incorporation of GO into ion gels as GPEs has not been reported so far.

In this work, a high-performance GO-doped ion gel (P(VDF-HFP)-EMIMBF₄-GO gel) was developed by exploiting the state-of-the-art ion gel system of P(VDF-HFP)-EMIMBF₄ with GO as the ionic conducting promoter. This GO-doped ion gel demonstrated significantly improved ionic conductivity compared with the pure ion gel without the addition of GO, due to the homogeneously distributed GO as a 3D network throughout the GO-doped ion gel by acting like an ion “highway” to facilitate the ion transport. Furthermore, the all-solid-state supercapacitor was fabricated and measured at room temperature using the GO-doped ion gel as GPE, which has demonstrated more superior electrochemical performance than the all-solid-state supercapacitor with pure ion gel and conventional supercapacitor with neat EMIMBF₄.

2. Results and Discussion

A series of GO-doped ion gels were prepared through a simple solution-mixing/casting method in anhydrous conditions as described in the experimental section. The products are denoted as P(VDF-HFP)-mEMIMBF₄-nwt%GO, where the “m” and “n” represent the mass ratio of EMIMBF₄/P(VDF-HFP) and the mass fraction of GO/P(VDF-HFP), respectively. **Figure 1a** displays a typical tapping-mode atomic-force microscopy (AFM) image of GO sheets used in this work. The size of most GO sheets are less than 500 nm and the corresponding high cross-sectional profile indicates that the height of most GO sheets are about 1.1 nm, which is characteristic of a single-layer GO sheet.^[26] **Figure 1b** shows the photographs of the resulting P(VDF-HFP)-2EMIMBF₄-GO gels with different GO

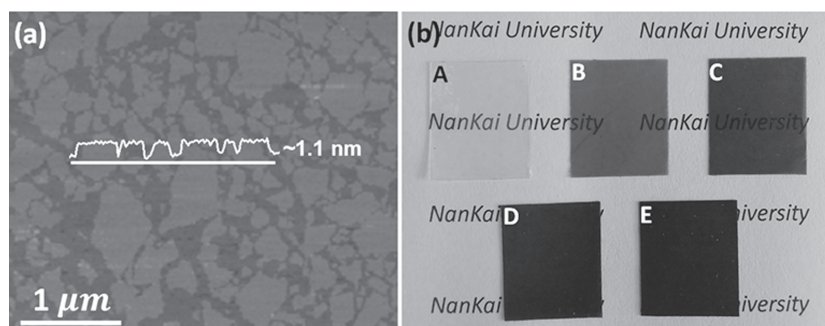


Figure 1. a) Typical tapping-mode atomic-force microscopy (AFM) image of GO sheets used in this work, which reveals that most GO sheets have heights of about 1.1 nm and sizes mainly less than 500 nm. b) Photographs of the obtained pure P(VDF-HFP)-2EMIMBF₄ gel (A), and P(VDF-HFP)-2EMIMBF₄-GO gels with GO doping mass fraction of 1 wt% (B), 2.5 wt% (C), 5 wt% (D), and 10 wt% (E), respectively.

doping mass fraction, and the pure P(VDF-HFP)-2EMIMBF₄ gel without the addition of GO as a comparison.

2.1. Properties of GO-Doped Ion Gels

The ionic conductivity of GO-doped ion gels was measured by electrochemical impedance spectroscopy (EIS) measurements with AC potential amplitude of 10 mV and a frequency range of 1 Hz–100 kHz. **Figure 2a** shows a typical Nyquist plot of impedance analysis on P(VDF-HFP)-2EMIMBF₄-1wt%GO gel. At high frequency (close to 100 kHz), the corresponding value of the intercept on the real axis (*x* axis) represents the intrinsic resistance of ion gel as the ohmic resistance of the testing device is negligible.^[40] The ionic conductivity is calculated according to the formula (1):

$$\sigma = \frac{L}{R \times S} \quad (1)$$

Where σ is the ionic conductivity, L is the distance between the two electrodes, R is the resistance of ion gels, and S is the geometric area of the electrode/electrolyte interface.

Based on the data obtained by impedance spectroscopy measurements, the ionic conductivity of P(VDF-HFP)-2EMIMBF₄-GO gels with different GO doping mass fraction is shown in **Figure 2b**. Interestingly, the addition of a small amount of GO into the ion gels results in a considerable increase in the ionic conductivity initially. Compared with that of pure P(VDF-HFP)-2EMIMBF₄ gel, only 1 wt% of GO doping makes a dramatic improvement of the ionic conductivity of about 260%. However, it is abruptly decreased with the excess addition of GO (more detailed discussion about this is presented below). Furthermore, the mass ratio of EMIMBF₄ and P(VDF-HFP) in ion gels also has great influence on the ionic conductivity. As shown in **Figure 2c**, the ionic conductivity is enhanced by increasing the mass ratio of EMIMBF₄ and P(VDF-HFP) from 1:1 to 1:5. However, further increasing the content of EMIMBF₄ in ion gel, the strength of the ion gel dramatically decrease and thus the samples can't meet the measurement demand. Overall, an optimized high ionic conductivity of about 25 mS cm⁻¹ was achieved in the sample of P(VDF-HFP)-5EMIMBF₄-1wt%GO gel, where

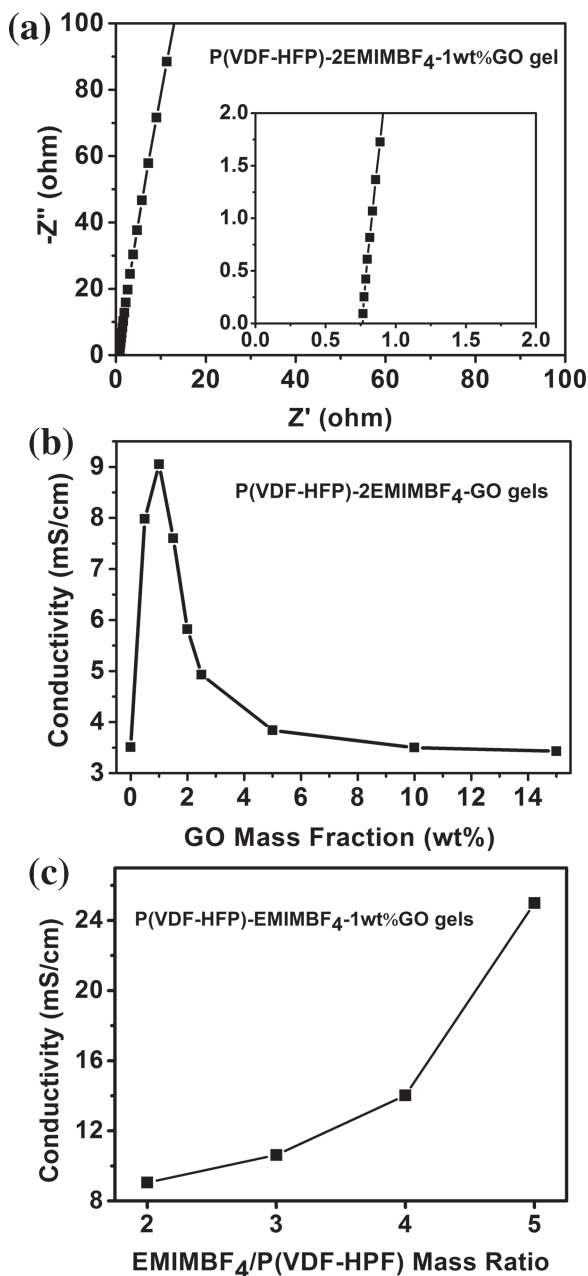


Figure 2. The ionic conductivity of GO-doped ion gels. a) Typical Nyquist plot of impedance analysis on P(VDF-HFP)-2EMIMBF₄-1wt%GO gel. The inset shows a magnified view of the high frequency region of the impedance spectra. b) Ionic conductivity of P(VDF-HFP)-2EMIMBF₄-GO gels with different GO doping mass fraction. c) Ionic conductivity of P(VDF-HFP)-EMIMBF₄-1wt%GO gels with different EMIMBF₄ and P(VDF-HFP) mass ratio.

the mass ratio of EMIMBF₄/P(VDF-HFP) is 5, the mass fraction of GO/P(VDF-HFP) is 1wt%, which is much higher than that of the pure P(VDF-HFP)-5EMIMBF₄ gel (11 mS cm⁻¹, Figure S1) and even slightly higher than the ionic conductivity of neat EMIMBF₄ (21 mS cm⁻¹, Figure S1). The increased ionic conductivity is believed due to the enhanced dissociation of the IL of EMIMBF₄ where GO acts as the additional dielectric

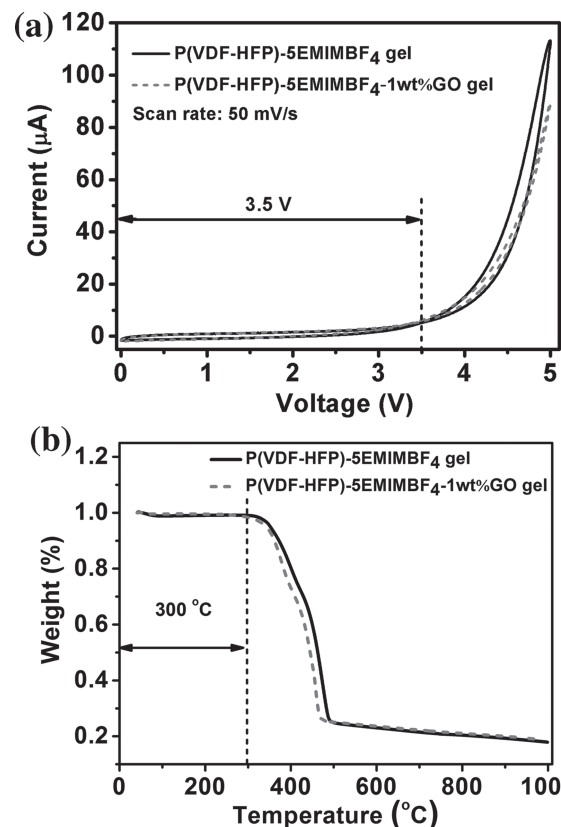


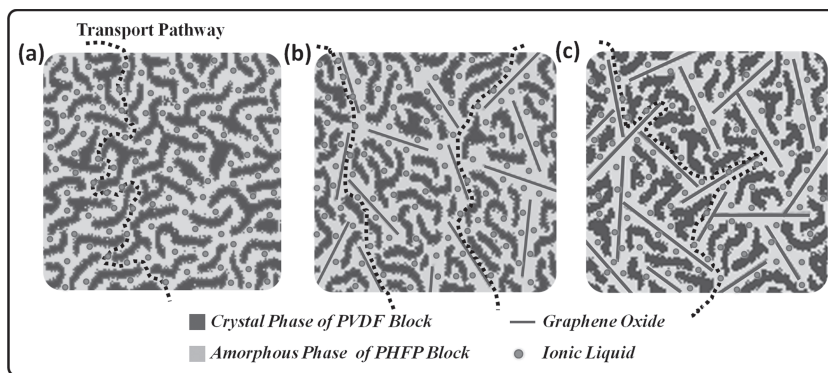
Figure 3. Electrochemical and thermal stability of pure P(VDF-HFP)-5EMIMBF₄ gel and P(VDF-HFP)-5EMIMBF₄-1wt%GO gel. a) Cyclic voltammogram at a potential scan rate of 50 mV s⁻¹ indicates that the ion gels are stable at a broad potential range of 0–3.5 V. b) Thermogravimetric analyses (TGA) thermogram under nitrogen atmosphere, with heating rate of 10 °C min⁻¹, demonstrates that the ion gels have excellent thermal stability.

substance^[6,41,42] and facilitates ion transport in the GO-doped ion gels as will be discussed below.

In order to operate at a broad potential window and temperature range, ion gels must have excellent electrochemical and thermal stability.^[15,43] The electrochemical and thermal stability of pure P(VDF-HFP)-5EMIMBF₄ gel and P(VDF-HFP)-5EMIMBF₄-1wt%GO gel are shown in Figure 3. Figure 3a shows the cyclic voltammograms of ion gels, measured at a potential scan rate of 50 mV s⁻¹. The rise of the current at high potential corresponds to the electrochemical reaction of ion gels. The cyclic voltammograms indicate that both pure P(VDF-HFP)-5EMIMBF₄ gel and P(VDF-HFP)-5EMIMBF₄-1wt%GO gel are stable at a broad potential range of 0–3.5 V, which is much higher than the aqueous (~1 V)^[7,9,10] and organic (~2.7 V)^[8] ion gels. Thermogravimetric analyses (TGA) thermogram of ion gels, shown in Figure 3b, demonstrates that both pure P(VDF-HFP)-5EMIMBF₄ gel and P(VDF-HFP)-5EMIMBF₄-1wt%GO gel have excellent thermal stability and are thermally stable below 300 °C. In addition, with the addition of GO, the P(VDFHFP)-5EMIMBF₄-1wt%GO gel has relatively lower thermal stability than the pure ion gel. It may be attributed to the interaction between GO and the copolymer P(VDF-HFP), which could decrease the crystallinity of copolymer thus result in a relatively lower thermal stability of the ion gel.^[44,45]

2.2. The Role of GO in GO-Doped Ion Gels

To interpret the effect of GO doping on ionic conductivity, we proposed the schematic structures of pure ion gel and GO-doped ion gels with different GO doping mass fractions (Scheme 1). The cross-section schematic structure of pure ion gel is shown in Scheme 1a. The crystal phase from crystalline part (PVDF) of copolymer maintains the mechanical property as the framework; while the amorphous phase mainly from the amorphous part (PHFP) acts as the entrapped channel for the supporting electrolyte (EMIMBF₄).^[15,16] The phase structure was examined using X-ray diffraction (XRD) characterization. As shown in Figure 4a, for the P(VDF-HFP) film, a strong diffraction peak is observed at the 2θ value of 20.4°, which corresponds to (200)/(110) reflections of the β-phase crystals of PVDF; a distinctive peak is also observed at the 2θ values of 18.5°, which corresponds to (020) reflection of the α-phase crystals of PVDF, indicating the coexistence of the α- and β-phases crystal of PVDF in P(VDF-HFP) film.^[46,47] Meanwhile, for the pure P(VDF-HFP)-2EMIMBF₄ gel and P(VDF-HFP)-2EMIMBF₄-GO gel with different GO doping mass fraction, the peak at 2θ value of 18.5° is weakened compared with that of the P(VDF-HFP) film, indicating that the α-phase crystals of PVDF is suppressed while the β-phase crystals of PVDF is slightly enhanced in the ion gels.^[46]



Scheme 1. Proposed cross-section schematic structures of GO-doped ion gels with different GO doping mass fraction. For easy presentation, the two dimensional (2D) graphene sheet is presented as a 1D line. a) Pure ion gel. b) GO-doped ion gel with optimized GO doping. c) GO-doped ion gel with excess GO dopings.

As the ions of EMIMBF₄ can only migrate through the disordered amorphous phase (transport pathway),^[15,16] which is demonstrated in Scheme 1a, thus the degree of crystalline should have a dramatically influence on the ionic conductivity. When the GO was added into the GO-doped ion gel, due to the abundant oxygen-containing functional groups on the surface and edge of GO sheets, the added GO should interact with the copolymer to form amorphous phase on the surface of GO and decrease the degree of crystalline in GO-doped ion gels. To demonstrate this, differential scanning calorimetry (DSC) was used to measure the melting enthalpy of pure P(VDF-HFP)-2EMIMBF₄ gel and P(VDF-HFP)-2EMIMBF₄-GO gel with different GO doping mass fraction, and the melt curves are shown in Figure 4b.

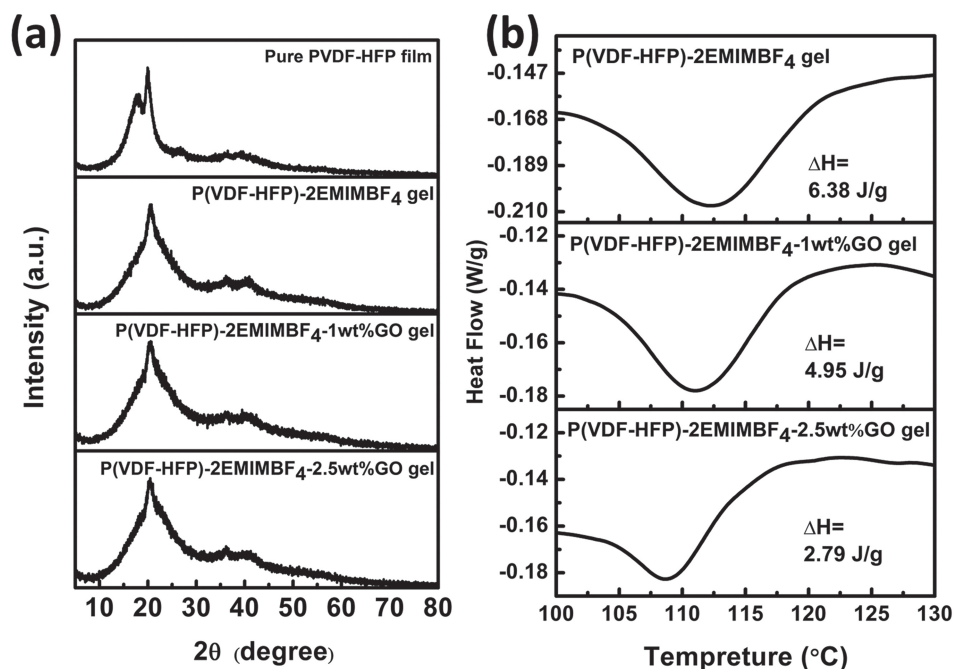


Figure 4. a) XRD pattern (plotted as Cu Kα) of P(VDF-HFP) film, pure P(VDF-HFP)-2EMIMBF₄ and P(VDF-HFP)-2EMIMBF₄-GO gels with different GO doping mass fraction. b) Differential scanning calorimetry (DSC) thermogram of pure P(VDF-HFP)-2EMIMBF₄ and P(VDF-HFP)-2EMIMBF₄-GO gels with different GO doping mass fraction. Compared with pure P(VDF-HFP)-2EMIMBF₄ gel, the melting peaks of P(VDF-HFP)-2EMIMBF₄-GO gels shift to lower temperature and the melting enthalpy value reduced with increasing the GO doping mass fraction, which indicates that the addition of GO indeed decrease the degree of crystalline in ion gel.

When increasing the doping mass fraction of GO, the melting peaks of GO-doped ion gels shift to left slightly from 112.5 °C for pure P(VDF-HFP)-2EMIMBF₄ gel to 108.5 °C for P(VDF-HFP)-2EMIMBF₄-2.5wt%GO gel, and the melting enthalpy value is also reduced from ΔH of 6.38 J g⁻¹ for pure P(VDF-HFP)-2EMIMBF₄ gel to 2.79 J g⁻¹ for P(VDF-HFP)-2EMIMBF₄-2.5wt%GO gel, which indicates that the addition of GO indeed decreases the degree of crystalline in GO-doped ion gels.^[48] Furthermore, due to the homogeneous distribution of GO as a 3D network in the ion gel matrix, a high degree of continuous and interconnected transport channel on the surface of GO can be formed (Scheme 1b), which can be described as “highway” for ion transport. Therefore, compared with that of pure ion gel, this “highway” built by 3D network of GO can result in higher ionic conductivity. Although the degree of crystalline in the GO-doped ion gel can be further reduced with more mass fraction of GO, the more addition of GO is expected to deteriorate the ionic conductivity due to the restacking of GO sheets and the blocking effect by the excessive GO as shown in Scheme 1c.

2.3. Electrochemical Performance of All-Solid-State Supercapacitor

Using the best recommended industry practice and method,^[49] an all-solid-state supercapacitor was fabricated by using the optimized GO-doped ion gel (P(VDF-HFP)-5EMIMBF₄-1wt%GO) as GPE and separator, a widely used commercial activated carbon RP20 as electrode material (SSA is about 1739 m² g⁻¹, the detail characterization of RP20 is shown in Supporting Information Figure S2). For comparison, another all-solid-state supercapacitor using pure ion gel (P(VDF-HFP)-5EMIMBF₄) as GPE and separator, and a conventional liquid supercapacitor using neat EMIMBF₄ as electrolyte were also fabricated using the same electrode material. Furthermore, all the electrochemical performances were studied at room-temperature.

Figure 5 shows the cyclic voltammetry comparison of all-solid-state supercapacitors with optimized GO-doped ion gel and pure ion gel, and conventional supercapacitor with neat EMIMBF₄ at low (25 mV s⁻¹) and high (200 mV s⁻¹) potential scan rates. At low potential scan rate of 25 mV s⁻¹, as shown in Figure 5a, all the curves are nearly rectangular, which is characteristic of an ideal capacitor;^[50] and the all-solid-state supercapacitor with optimized GO-doped ion gel shows almost the same capacitance performance as the conventional supercapacitor with neat EMIMBF₄, but much higher than that of all-solid-state supercapacitor with pure ion gel. However, at high potential scan rate of 200 mV s⁻¹, as shown in Figure 5b, all the curves start to become distorted as the overall internal resistance of the devices becomes a dominant factor;^[42] nevertheless, the curve of all-solid-state supercapacitor with optimized GO-doped ion gel is less distorted and the capacitance performance is higher than the other two devices. These results confirm that the all-solid-state supercapacitor with optimized GO-doped ion gel has lower internal resistance, which would be beneficial to get higher specific capacitance and better power performance.

The capacitance performances at various charge/discharge current densities were measured through galvanostatic charge/discharge measurements. Figure 6a shows the specific

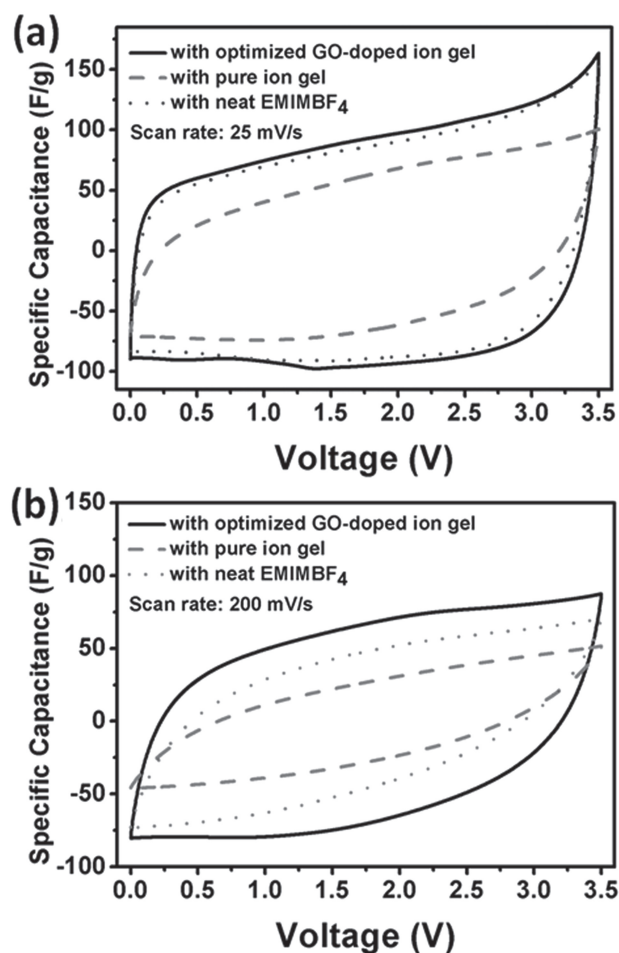


Figure 5. Comparison of cyclic voltammetry measurements of all-solid-state supercapacitors with optimized GO-doped ion gel and pure ion gel, and conventional supercapacitor with neat EMIMBF₄ at potential scan rates of a) 25 mV s⁻¹ and b) 200 mV s⁻¹.

capacitance values at various discharge current densities. At low discharge current density, the specific capacitance of the all-solid-state supercapacitor with optimized GO-doped ion gel is only a little higher than that of conventional supercapacitor with neat EMIMBF₄ and all-solid-state supercapacitor with pure ion gel. However, when increasing current densities, its specific capacitance is getting much higher than the other two devices, again indicating a lower internal resistance than the other two devices. Figure 6b shows the galvanostatic charge/discharge curves at a current density of 1 A g⁻¹. All the curves are nearly straight lines, which means that the all-solid-state supercapacitors with optimized GO-doped ion gel and pure ion gel have the standard capacitive behavior of double layer capacitors as the conventional supercapacitor.^[51] In galvanostatic charge/discharge measurements, the voltage drop appeared at the beginning of the discharge is associated with the overall internal resistance of devices. Figure 6c summarizes the variation of voltage drop with different current densities. The voltage drop increases linearly with the increase of current density for each device, and the slope of this linear relationship corresponds to the overall internal resistance value.^[52] As shown in Figure 6c,

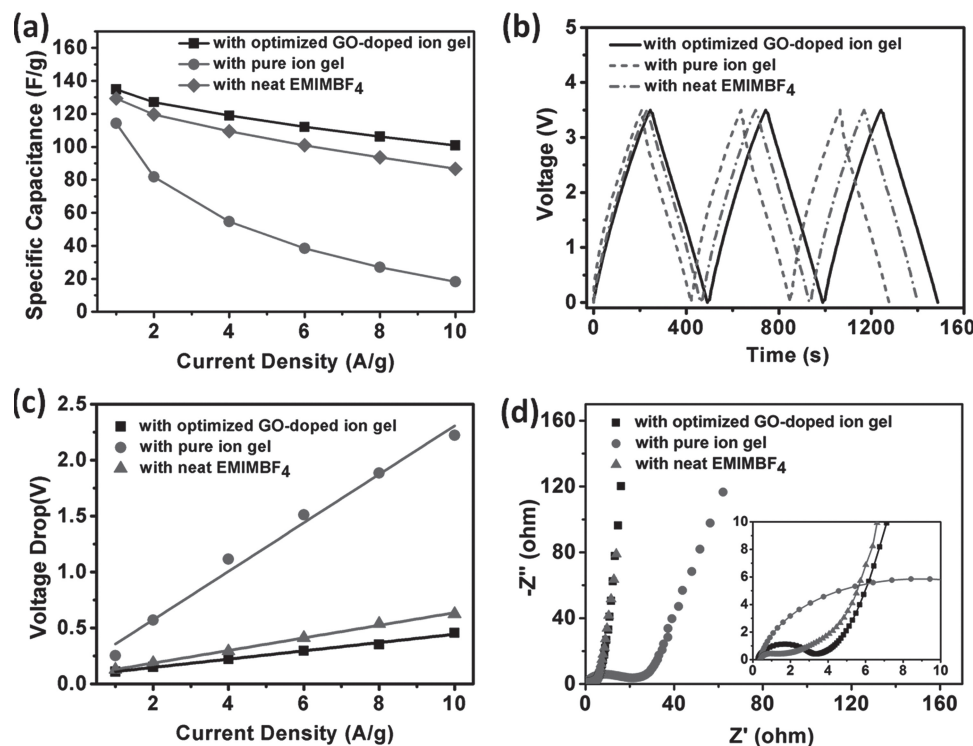


Figure 6. Electrochemical performance characterization of all-solid-state supercapacitors with optimized GO-doped ion gel and pure ion gel, and conventional supercapacitor with neat EMIMBF₄. a) Specific capacitances at various discharge current densities. b) Typical galvanostatic charge/discharge curves at a current density of 1 A g⁻¹. c) Voltage drop associated with the internal resistance of device at different discharge current densities. d) Nyquist impedance plots at a frequency range of 10 mHz to 100 kHz. The inset shows a magnified view of the high frequency region of the impedance spectra.

the overall internal resistance of the all-solid-state supercapacitor with optimized GO-doped ion gel is a little lower than that of conventional supercapacitor with neat EMIMBF₄, but much lower than that of all-solid-state supercapacitor with pure ion gel. This lower internal resistance would contribute greatly to the higher specific capacitance and better power performance for the optimized GO-doped ion gel based all-solid-state supercapacitor.

Nyquist plots of the all-solid-state supercapacitors with optimized GO-doped ion gel and pure ion gel, and conventional supercapacitor with neat EMIMBF₄, were obtained by a frequency response analysis (FRA) of the frequency range from 10 mHz to 100 kHz. The Nyquist plots show a typical response of a porous electrode, as shown in Figure 6d with an expanded view provided in the inset. The Nyquist plots exhibit an intercept on the real axis (x axis) at high frequency (close to 100 kHz), which represents the intrinsic internal resistance of the electrode material and electrolyte of device, a approximate semicircular behavior at the high to midfrequency region, which is related to the interface nature of electrolyte and electrode material, a 45° Warburg region at the middle frequency region, which is related to the diffusion of the ions into the bulk of electrodes, and an almost vertical line at low frequencies, indicating the ideal capacitive performance of device.^[40,53] As shown in Figure 6d, all the devices have the similar intercept on the real axis at high frequency, which means that the intrinsic internal resistance of the electrode material and electrolyte is not the

major determinant for the overall internal resistance of devices. Compared with the Nyquist plots of the devices with optimized GO-doped ion gel and neat EMIMBF₄, the Nyquist plots of the all-solid-state supercapacitor with pure ion gel exhibits a much larger diameter of semicircular at the high to midfrequency region, which indicates a very poor connected interface nature of pure ion gel and electrode material, which mainly decided the overall internal resistance. This result demonstrates the pivotal role of GO for improving the interface nature of ion gel and electrode material compared with that of pure ion gel. In addition, the all-solid-state supercapacitor with optimized GO-doped ion gel has a relatively shorter 45° Warburg region at the middle frequency, and a more vertical line at low frequencies, which indicates that the device has much better electrochemical performance and also confirms that the GO-doped ion gel has higher ionic conductivity and much better compatibility with carbon electrodes than the pure ion gel and neat EMIMBF₄.

Ragone plots (power density vs. energy density) for the all-solid-state supercapacitor with optimized GO-doped ion gel and compared with that of conventional supercapacitor with neat EMIMBF₄ are shown in Figure 7a. From the Ragone plots, the application of optimized GO-doped ion gel improves the all-solid-state supercapacitor performance and preserves the energy at high power density. The energy density can reach as high as 32.4 Wh kg⁻¹ for the all-solid-state supercapacitor at a power density of 6.6 kW kg⁻¹ at a current density of 10 A g⁻¹. In comparison, at the same current density of 10 A g⁻¹, the

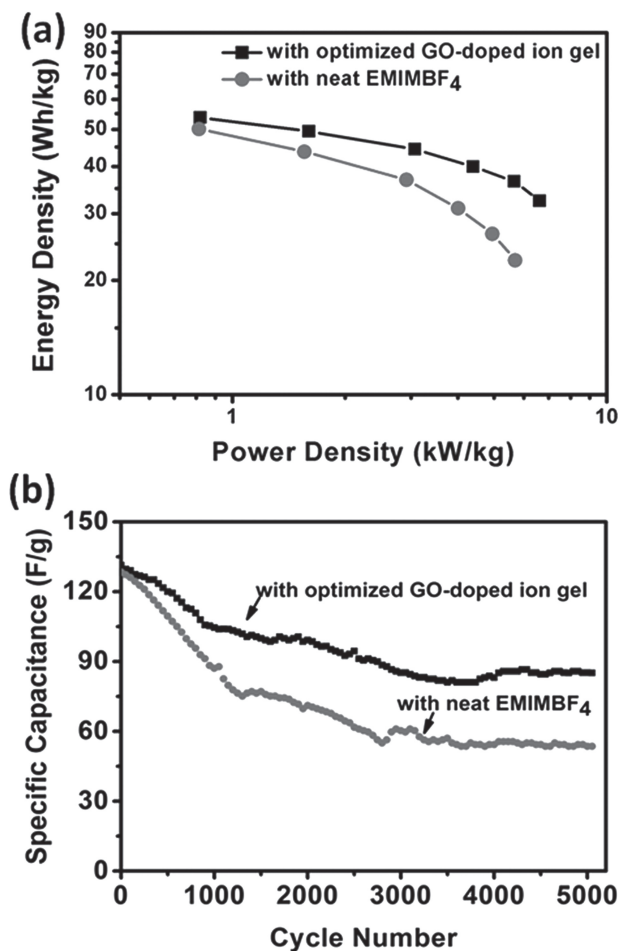


Figure 7. a) Ragone plots of the all-solid-state supercapacitors with optimized GO-doped ion gel, and conventional supercapacitor with neat EMIMBF₄. b) The cycling performance of the all-solid-state supercapacitors with optimized GO-doped ion gel, and conventional supercapacitor with neat EMIMBF₄ at a charge/discharge current density of 1 A g⁻¹.

energy density and power density are only 22.6 Wh kg⁻¹ and 5.7 kW kg⁻¹ respectively for the conventional supercapacitor. The GO-doped ion gel evidently facilitates charge storage and ionic transport in the device system. Moreover, the cycling performance was also measured for the all-solid-state supercapacitors with optimized GO-doped ion gel and conventional supercapacitor with neat EMIMBF₄ at a current density of 1 A g⁻¹, as shown in Figure 7b. Due to the high ionic conductivity and excellent compatibility with carbon electrodes of the optimized GO-doped ion gel, the all-solid-state supercapacitor exhibits better cycle stability than the conventional supercapacitor.

3. Conclusions

In summary, GO, as a ionic conducting promoter for ion gel, has been demonstrated for the first time to dramatically improve the ionic conductivity of GO-doped ion gel compared with that of pure ion gel. Due to the homogeneous distribution of GO as a 3D network in GO-doped ion gels, a high

degree of continuous and interconnected transport channel was developed to facilitate the ion transport and resulted in a considerable increase in the ionic conductivity. Furthermore, compared with the all-solid-state supercapacitor with pure ion gel and conventional supercapacitor with neat EMIMBF₄, the all-solid-state supercapacitor with optimized GO-doped ion gel has more superior electrochemical performance in the aspect of smaller internal resistance, higher capacitance performance, and better cycle stability. These excellent properties are attributed to the high ionic conductivity, excellent compatibility with carbon electrodes, and long-term stability of GO-doped ion gel. We believe that the excellent performance of P(VDF-HFP)-EMIMBF₄-GO gels may bring new design opportunities of device configuration for energy-storage devices in the future wearable electronics field.

4. Experimental Section

Go-Doped Ion Gels Preparation: A series of P(VDF-HFP)-EMIMBF₄-GO gels were obtained using a simple solution-mixing/casting method according to different GO loading mass fraction and different mass ratio of EMIMBF₄ and P(VDF-HFP). Typically, the synthesis procedure for a typical P(VDF-HFP)-2EMIMBF₄-1wt%GO gel was as follows: GO (6 mg, Tianjin Plannano Co., Ltd.) was dispersed in DMF (6 g, >99% purity, Tianjin Guangfu Co., Ltd) in an ultrasonic bath to obtain a clear solution. Then, copolymer P(VDF-HFP) (600 mg, Solvay Solexis) and EMIMBF₄ (1.2 g, Lanzhou Kaite trade co., Ltd) were added to the GO/DMF solution to form a homogeneous viscous mixture under vigorous stirring. Finally, this homogeneous viscous solution was cast onto an aluminum substrate (8 cm × 8 cm) to evaporate the DMF at 80 °C for 12 h, and the resulting P(VDF-HFP)-2EMIMBF₄-1wt%GO gel film was finally peeled off of the substrate and punched into a round film with diameter of 1.8 cm for further testing.

Characterization: Typical tapping-mode atomic force microscopy (AFM) was taken using multimode SPM from digital instruments with a Nanoscope IIIa controller. X-ray diffraction (XRD) measurements were performed on a Rigaku D/Max-2500 diffractometer with Cu K α radiation. The degree of crystallinity of the samples was investigated by differential scanning calorimetry (DSC) using a NETZSCH STA-409PC instrument. Thermo gravimetric analysis (TGA) was also carried out for thermal stability measurement using a NETZSCH STA-409PC instrument. The testing device for ionic conductivity and electrochemical stability characterization is constituted by sandwiching the rounded GO-doped ion gel (diameter of 1.8 cm) with two rounded aluminum foils (diameter of 1.5 cm). The electrochemical impedance spectroscopy (EIS) measurements and cyclic voltammetry (CV) analysis were carried out using the Autolab (Metrohm).

Fabrication of All-Solid-State Supercapacitor: Briefly, 80 wt% commercial activated carbon RP20 (Kuraray Chemicals), 10 wt% PTFE (Dupont) and 10 wt% carbon black (Super P, Timcal) were homogeneously mixed and rolled into 100-120 μ m thickness sheets, and then punched into round electrodes with diameter of 1.5 cm. After dried at 120 °C for 6 h under vacuum, the electrodes were weighted and hot pressed onto the current collectors (aluminum foils with conducting carbon coating, Tianjin Lishen Co., Ltd.) and then dried at 180°C for 6 h under high vacuum to completely remove water. The dry working electrodes (5–7 mg) were transferred into a glove box filled with Ar to construct the all-solid-state supercapacitors and conventional supercapacitors. All-solid-state supercapacitors consist of two working electrodes using the optimized GO-doped ion gel or pure ion gel as GPEs and separators, while the conventional supercapacitor consist of two working electrodes and a separator (TF4840, NKK) using neat EMIMBF₄ as electrolyte.

Measurement of All-Solid-State Supercapacitor: All the electrochemical tests were carried out at room temperature. Galvanostatic charge/

discharge tests at various current densities and cycle stability of cells were measured using an Arbin testing system (Arbin MSTAT, America). The gravimetric specific capacitance, C_s ($F\ g^{-1}$), was calculated according to formula (2):

$$C_s = \frac{4I}{mdV/dt} \quad (2)$$

where I is the constant current (A), m is the total mass of two electrodes (g), dV/dt ($V\ s^{-1}$) is the slope obtained by fitting a straight line to the discharge curve.

The energy density, E_{cell} ($Wh\ kg^{-1}$), was estimated using the formula (3):

$$E_{cell} = C_s V^2 / 8 \quad (3)$$

and, the power density, P_{cell} ($kW\ kg^{-1}$), was calculated according to the formula (4):

$$P_{cell} = E_{cell} / \Delta t \quad (4)$$

where the V is the discharge voltage, Δt is the discharge time.

Cyclic voltammetry (CV) and electrical impedance spectroscopy (EIS) studies were performed using Autolab (Metrohm). CV tests were carried out in various scan rates; EIS measurements were carried out with AC potential amplitude of 10 mV and a frequency range of 10 mHz–100 kHz.

Supporting Information

Supporting Information is available from the Wiley Online Library or from the author.

Acknowledgements

The authors gratefully acknowledge financial support from MoST (Grants 2012CB933401, 2011CB932602 and 2011DFB50300), NSFC (Grants 50933003, 50902073 and 50903044).

Received: December 2, 2012

Published online: February 6, 2013

- [1] H. Nishide, K. Oyaizu, *Science* **2008**, 319, 737.
- [2] J. R. Miller, *Science* **2012**, 335, 1312.
- [3] *Polymer Electrolyte Reviews 1 and 2* (Eds: J. R. MacCallum, C. A. Vincent) Elsevier, London **1987**.
- [4] Md. A. B. H. Susan, T. Kaneko, A. Noda, M. Watanabe, *J. Am. Chem. Soc.* **2005**, 127, 4976.
- [5] J. M. Tarascon, M. Armand, *Nature* **2001**, 414, 359.
- [6] F. Croce, G. B. Appetecchi, L. Persi, B. Scrosati, *Nature* **1998**, 394, 456.
- [7] C. Meng, C. Liu, L. Chen, C. Hu, S. Fan, *Nano Lett.* **2010**, 10, 4025.
- [8] T. Osaka, X. J. Liu, M. Nojima, T. Momma, *J. Electrochem. Soc.* **1999**, 146, 1724.
- [9] M. Kaempgen, C. K. Chan, J. Ma, Y. Cui, G. Gruner, *Nano Lett.* **2009**, 9, 1872.
- [10] L. Hu, M. Pasta, F. La Mantia, L. Cui, S. Jeong, H. D. Deshazer, J. W. Choi, S. M. Han, Y. Cui, *Nano Lett.* **2010**, 10, 708.
- [11] Y. J. Kang, S. J. Chun, S. S. Lee, B. Y. Kim, J. H. Kim, H. Chung, S. Y. Lee, W. Kim, *ACS Nano* **2012**, 6, 6400.
- [12] B. G. Choi, J. Hong, W. H. Hong, P. T. Hammond, H. Park, *ACS Nano* **2011**, 5, 7205.
- [13] A. M. Stephan, *Euro. Poly. J.* **2006**, 42, 21.
- [14] C. C. Yang, *J. Power Sources* **2002**, 109, 22.
- [15] V. K. Thakur, G. Ding, J. Ma, P. S. Lee, X. Lu, *Adv. Mater.* **2012**, 24, 4071.
- [16] T. P. Lodge, *Science* **2008**, 321, 50.
- [17] W. Lu, K. Henry, C. Turchi, J. Pellegrino, *J. Electrochem. Soc.* **2008**, 155, A361.
- [18] H. Y. Sung, Y. Y. Wang, C. C. Wan, *J. Electrochem. Soc.* **1998**, 145, 1207.
- [19] M. Armand, F. Endres, D. R. MacFarlane, H. Ohno, B. Scrosati, *Nat. Mater.* **2009**, 8, 621.
- [20] P. Bonhote, A. P. Dias, M. Armand, N. Papageorgiou, K. Kalyanasundaram, M. Gratzel, *Inorg. Chem.* **1998**, 37, 166.
- [21] P. Simon, Y. Gogotsi, *Nat. Mater.* **2008**, 7, 845.
- [22] P. Simon, Y. Gogotsi, *Acc. Chem. Res.* **2012**, DOI:10.1021/ar200306b.
- [23] G. B. Appetecchi, P. Romagnoli, B. Scrosati, *Electrochem. Comm.* **2001**, 3, 281.
- [24] D. Saikia, A. Kumar, *Euro. Poly. J.* **2005**, 41, 563.
- [25] M. Wachtler, D. Ostrovskii, P. Jacobsson, B. Scrosati, *Electrochim. Acta* **2004**, 50, 357.
- [26] Y. Zhu, S. Murali, W. Cai, X. Li, J. W. Suk, J. R. Potts, R. S. Ruoff, *Adv. Mater.* **2010**, 22, 3906.
- [27] D. Chen, H. Feng, J. Li, *Chem. Rev.* **2012**, 112, 6027.
- [28] X. Huang, X. Qi, F. Boey, H. Zhang, *Chem. Soc. Rev.* **2012**, 41, 666–686.
- [29] X. Huang, Z. Yin, S. Wu, X. Qi, Q. He, Q. Zhang, Q. Yan, F. Boey, H. Zhang, *Small* **2011**, 7, 1876–1902.
- [30] X. Huang, Z. Zeng, Z. Fan, J. Liu, H. Zhang, *Adv. Mater.* **2012**, 24, 5979–6004.
- [31] Q. He, S. Wu, Z. Yin, H. Zhang, *Chem. Sci.* **2012**, 3, 1764–1772.
- [32] Y. S. Ye, C. Y. Tseng, W. C. Shen, J. S. Wang, K. J. Chen, M. Y. Cheng, J. Rick, Y. J. Huang, F. C. Chang, B. J. Hwang, *J. Mater. Chem.* **2011**, 21, 10448.
- [33] C. Tang, K. Hackenberg, Q. Fu, P. M. Ajayan, H. Ardebili, *Nano Lett.* **2012**, 12, 1152.
- [34] X. Cao, Y. Shi, W. Shi, G. Lu, X. Huang, Q. Yan, Q. Zhang, H. Zhang, *Small* **2011**, 7, 3163–3168.
- [35] Y. Wang, Z. Shi, Y. Huang, Y. Ma, C. Wang, M. Chen, Y. Chen, *J. Phys. Chem. C* **2009**, 113, 13103–13107.
- [36] M. D. Stoller, S. Park, Y. Zhu, J. An, R. S. Ruoff, *Nano Lett.* **2008**, 8, 3498–3502.
- [37] Y. Xu, K. Sheng, C. Li, G. Shi, *ACS Nano* **2010**, 4, 4324–4330.
- [38] W. Lv, D. M. Tang, Y. B. He, C. H. You, Z. Q. Shi, X. C. Chen, C. M. Chen, P. X. Hou, C. Liu, Q. H. Yang, *ACS Nano* **2009**, 3, 3730–3736.
- [39] Y. Wu, T. Zhang, F. Zhang, Y. Wang, Y. Ma, Y. Huang, Y. Liu, Y. Chen, *Nano Energy* **2012**, 1, 820–827.
- [40] P. L. Taberna, P. Simon, J. F. Fauvarque, *J. Electrochem. Soc.* **2003**, 150, A292.
- [41] M. Ishikawa, M. Morita, M. Ihara, Y. Matsuda, *J. Electrochem. Soc.* **1994**, 141, 1730.
- [42] C. Huang, C. Wu, Sh. Hou, P. Kuo, Ch. Hsieh, H. Teng, *Adv. Fun. Mater.* **2012**, 22, 4677.
- [43] J. Jiang, D. Gao, Z. Li, G. Su, *React. Funct. Polym.* **2006**, 66, 1141.
- [44] S. L. Qiu, C. S. Wang, Y. T. Wang, C. G. Liu, X. Y. Chen, H. F. Xie, Y. A. Huang, R. S. Cheng, *Express Poly. Lett.* **2011**, 5, 809.
- [45] B. J. Chae, D. H. Kim, I. S. Jeong, J. R. Hahn, B. Ch. Ku, *Carbon Lett.* **2012**, 13, 221.
- [46] N. Levi, R. Czerw, S. Y. Xing, P. Iyer, D. L. Carroll, *Nano Lett.* **2004**, 4, 1267.
- [47] L. Zhang, D. a. Zha, T. Du, S. Mei, Z. Shi, Z. Jin, *Langmuir* **2011**, 27, 8943.
- [48] J. Liang, Y. Huang, L. Zhang, Y. Wang, Y. Ma, T. Guo, Y. Chen, *Adv. Funct. Mater.* **2009**, 19, 2297.
- [49] Y. Gogotsi, P. Simon, *Science* **2011**, 334, 917.
- [50] E. Frackowiak, F. Beguin, *Carbon* **2001**, 39, 937.
- [51] C. Liu, Z. Yu, D. Neff, A. Zhamu, B. Z. Jang, *Nano Lett.* **2010**, 10, 4863.
- [52] A. Izadi-Najafabadi, S. Yasuda, K. Kobashi, T. Yamada, D. N. Futaba, H. Hatori, M. Yumura, S. Iijima, K. Hata, *Adv. Mater.* **2010**, 22, E235.
- [53] B. G. Choi, M. Yang, W. H. Hong, J. W. Choi, Y. S. Huh, *ACS Nano* **2012**, 6, 4020.